Ocean Dynamics
DOI 10.1007/s10236-015-0830-1

Why is there net surface heating over the Antarctic Circumpolar Current?

Arnaud Czaja · John Marshall

Received: 27 October 2014 / Accepted: 4 March 2015

Abstract Using a combination of atmospheric reanalysis data, climate model outputs and a simple model, key mechanisms controlling net surface heating over the Southern Ocean are identified. All data sources used suggest that, in a streamline-averaged view, net surface heating over the Antarctic Circumpolar Current (ACC) is a result of net accumulation of solar radiation rather than a result of heat gain through turbulent fluxes (the latter systematically cool the upper ocean). It is proposed that the fraction of this net radiative heat gain realized as net ACC heating is set by two factors. First, the sea surface temperature at the southern edge of the ACC. Second, the relative strength of the negative heatflux feedbacks associated with evaporation at the sea surface and advection of heat by the residual flow in the oceanic mixed layer. A large advective feedback and a weak evaporative feedback maximize net ACC heating. It is shown that the present Southern Ocean and its circumpolar current are in this heating regime.

Responsible Editor: Jinyu Sheng

This article is part of the Topical Collection on *Atmosphere and Ocean Dynamics: A Scientific Workshop to Celebrate Professor Dr. Richard Greatbatch's 60th Birthday, Liverpool, UK, 10-11 April 2014*

A. Czaja (✉)
Department of Physics, Imperial College, Prince Consort Road, London SW7 2AZ, England
e-mail: a.czaja@imperial.ac.uk

J. Marshall
Department of Earth, Atmospheric and Planetary Sciences, Massachusetts Institute of Technology, 77 Massachusetts Avenue, Cambridge, MA 02139, USA
e-mail: jmarsh@mit.edu

Keywords Antarctic Circumpolar Current · Air-sea heat flux negative feedback

1 Introduction

The global ocean circulation is associated with the transformation of warm waters to cold waters in poleward flowing currents. To maintain a steady state, the reverse transformation, from cold to warm must occur (Walin 1982). The relative importance of air-sea fluxes and interior diffusive processes in this transformation is still uncertain and much debated. Indeed, it is one of the most central and long-standing questions in physical oceanography, as reviewed in Wunsch and Ferrari (2004). One possible scenario is that sinking in northern Atlantic polar latitudes triggered by heat loss is balanced by warming at the sea surface of the Southern Hemisphere due to air-sea interaction, with interior mixing playing a secondary role (see for instance Toggweiler and Samuels 1998; Gnanadesikan 1999; Howe and Czaja 2009 and the review by Marshall J and Speer 2012).

Of crucial importance for the surface diabatic mechanism is that large-scale ocean-atmosphere interactions can sustain a net heating of the ocean over the cold waters of the Southern Ocean. Various estimates based on "bulk-formulae" (Taylor et al. 1978; Grist and Josey 2003) and global ocean inversions (e.g., Ganachaud and Wunsch 2000) support the view that there is Southern Ocean heating (see for example, Fig. 1), although the precise magnitude and geographical extent has considerable uncertainty.

From the point of the view of the oceanographer, Southern Ocean heating is no surprise and is understood as a required feature of the meridional circulation of the Southern Ocean, the so-called "diabatic Deacon cell" (Speer et al.

Published online: 31 March 2015

2000). Water parcels upwell in the Antarctic divergence south of the Antarctic Circumpolar Current (ACC), move equatorward in the upper Ekman layer, and thus experience a temperature increase as they cross the ACC front. This requires net surface heating in the time mean. Budgets reveal that the magnitude of the heating is consistent with the strength of the circulation and the temperature change across the ACC temperature front (see, e.g, Marshall 1997, Speer et al. 2000, Badin and Williams 2010).

Despite the soundness of this argument, it is still somewhat of a surprise to observe surface heating of the ocean at latitudes as far south as 40–60° S. Taylor et al. (1978) suggest that this can be understood as the result of warm, moist advection of air by weather disturbances from the subtropics over cold ocean waters. Speer et al. (2000) emphasized the zonal asymmetry of the heating, with most of it being concentrated over the Atlantic-Indian sector where the ACC is most displaced equatorward. Again, cold waters under warm air is invoked to explain the heating.

An obvious criticism of these arguments is that sensible and latent heat fluxes usually cool the ocean surface and it is only the net radiative component of the surface flux which provides heating (Csanady 2001). As we shall see, all datasets considered below indeed show that accumulation of solar radiation, rather than warm moist advection by the atmosphere, is the primary driver of the net heating of the ACC. The warm moist advection by the atmosphere can contribute to reducing the sensible and evaporative cooling, but we suggest here that this reduction is primarily controlled, in a streamline averaged sense, by the northward advection of cold water by the residual flow in the oceanic mixed layer.

The paper is structured as follows. In Section 2, we analyze the various components of the net surface heat flux over the Southern Ocean in a reanalysis dataset and show that net heating essentially reflects a small residual between radiative heating and evaporative cooling. This approximate balance is also found to hold in idealised coupled climate simulations described in Section 3. A simple model to explore processes controlling the net air-sea heat flux over the ACC is then developed and studied in Section 4. Our discussion and conclusions are presented in Section 5.

2 Surface heating in reanalysis data

The net surface heat flux Q_{net} at the air-sea interface can be decomposed into the sum of net radiative heating Q_{rad} (itself the sum of the net shortwave solar heating and the net longwave cooling, $Q_{rad} = Q_{lw} + Q_{sw}$), sensible Q_{sen} and latent heat flux Q_{lat}, here all taken to be positive downwards:

$$Q_{net} = Q_{rad} + Q_{sen} + Q_{lat}. \quad (1)$$

Figure 1 depicts the annual-mean value of Q_{net} (in Wm^{-2}) over the Southern Ocean, estimated from the NCEP-NCAR reanalysis (Kalnay and et al. 1996) over the 1980–2012 period. The net heat flux reflects a small residual between ocean heat gain in the summer and ocean heat loss in the winter (not shown). One observes that over most of the ocean $Q_{net} \approx 0$, except (i) near the Aguhlas region, the Malvinas confluence region and over the East Australian current where a net cooling of a few tens of Wm^{-2} is found (ii) over a spiraling band originating on the poleward side of the Malvinas confluence region, stretching all across the Atlantic basin and ending toward the middle of the Indian Ocean, where net heating of a few tens of Wm^{-2} is observed.

This latter band of heating is strikingly coincident with the path of the ACC over the Atlantic and Indian basins, as indicated by the magenta contours in Fig. 1. These are lines of constant ocean mean dynamic topography, −60 and −130 cm for the northern and southern edge, respectively, taken from the climatological estimate of Maximenko et al. 2009 (their estimate following "method C"). For future reference, the time mean SST of the ACC within this band is 3.9 °C while, for the northern and southern boundaries it is 6.6 and 1.1 °C, respectively (the SST data used here is that from the NCEP-NCAR reanalysis). Indeed, although the ACC is roughly centred on the 45° S–60° S latitude band, the net heating is found to be 30 % larger (28 Wm^{-2} as opposed to 20 Wm^{-2}) when averaged between the streamlines in Fig. 1 rather than between the 45 and 60° latitude circles (Table 1, compare second and third columns).

To understand the origin of the net heating, we decompose Q_{net} according to Eq. 1, and sum each component over

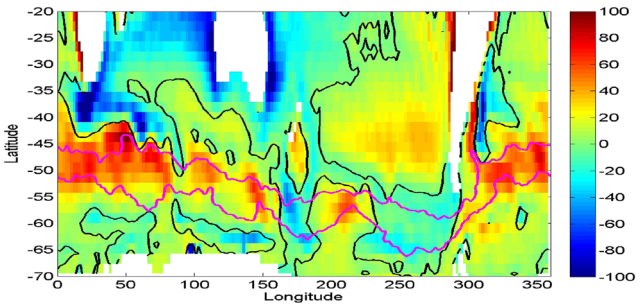

Fig. 1 Annual mean net surface heat flux (in Wm^{-2}, positive into the ocean, zero contour highlighted in *black*) over the Southern Ocean, with the ACC band delimited by the two *magenta lines*. Q_{net} is taken from the NCEP-NCAR reanalysis while the ACC path is defined using the data of Maximenko et al. (2009)

Table 1 Components of the air-sea flux (in Wm^{-2}) and sea surface temperature (SST, in °C) over the Southern Ocean

Averaging	ACC streamline	45° S–60° S	45° S–55° S	45° S–55° S
Data source	NCEP-NCAR reanalysis	NCEP-NCAR reanalysis	MITgcm "Aquaplanet"	MITgcm "Double Drake"
Q_{net}	+28	+20	−4	+4
Q_{sen}	−1	−4	−14.8	−15.9
Q_{lat}	−30	−35	−60.9	−47.6
Q_{rad}	+59	+59	+71.6	+67.5
SST	3.9	4.6	15.3	11.4

The second and third columns refer to reanalysis data while the last two on the right refer to the idealized climate simulations

longitudinal bins extending meridionally between the two ACC streamlines shown in Fig. 1. The result is expressed in Wm^{-2} by dividing by the area of the bins, as displayed in Fig. 2. It is seen that the main heat balance is between net radiative heat gain ($Q_{rad} > 0$, red) and evaporative cooling ($Q_{lat} < 0$, dark blue), the sensible heat flux playing a lesser role. Averaged over all longitudes, the net heating of 28 Wm^{-2} mentioned previously is the result of a net radiative heat gain of 59 Wm^{-2} and an evaporative cooling of 30 Wm^{-2} (Table 1, second column). A similar leading order balance is obtained when averaging over 45–60° S but, interestingly, the turbulent heat fluxes (Q_{sen} and Q_{lat}) increase significantly in this case while radiative heating remains similar (Table 1, third column). This suggests that by following the ACC, one reduces the thermodynamic imbalance between the ocean and the lower atmosphere, thus reducing the contribution of turbulent heat fluxes.

3 Surface heating in a coupled model

We now turn to analyzing the air-sea heat fluxes simulated in a coupled climate model of intermediate complexity. This couples a coarse version of the MIT ocean model (run on a cubed sphere at a resolution of C24, i.e., 24 × 24 points per face, yielding a resolution of 3.75° at the equator, 15 vertical levels) to a five-layer atmospheric model with same hydrodynamical core (Marshall J et al. 1997, Marshall J et al. 2004) and simplified physics (Molteni 2003) run in idealized planetary geometries. We focus here on the "Aquaplanet" (no land at all) and the "Double-Drake" (two submarine ridges extending through the full depth of the ocean and ranging meridionally from 90° N to 35° S and set 90° of longitude apart) simulations, both run with a flat ocean bottom. Note that the ocean and the atmosphere share the same horizontal grid. Simplified parameterizations of subgrid scale physics are used, as described in Enderton and Marshall (2009) and Ferreira et al. (2010). All averages shown are constructed from the last 50 years of the long equilibrium solutions discussed in Ferreira et al. (2010). The reader is referred to this paper for more information about the model.

The SST simulated in the Southern Hemisphere in the Aquaplanet and the Double-Drake geometries is shown in Fig. 3 (left panel, solid and dashed lines, respectively). It is seen that the introduction of a North-South asymmetry in the Double-Drake geometry introduces a dramatic cooling of several degrees in the Southern Hemisphere. This cooling is associated with a deep meridional overturning and its South-to-North heat transport. Indeed, while the Southern Hemisphere SSTs drop, Northern Hemisphere SSTs

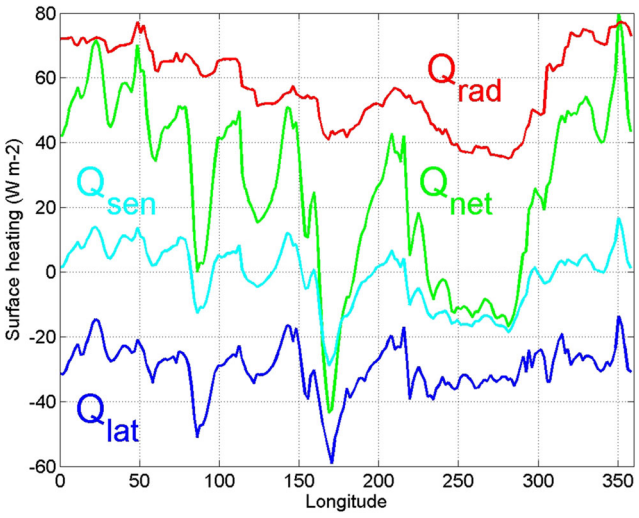

Fig. 2 Annual mean net surface heat flux (Q_{net} in *green*), net radiative heat gain (Q_{rad} in *red*), sensible (Q_{sen} in *light blue*) and latent heat flux (Q_{lat} in *dark blue*) along the path of the ACC. The fluxes are all given in Wm^{-2}, and are computed by summing over bins of longitude extending meridionally between the two ACC streamlines shown in black in Fig. 1, and further dividing by the area of the bins. Negative terms cool the ocean while positive terms heat the ocean

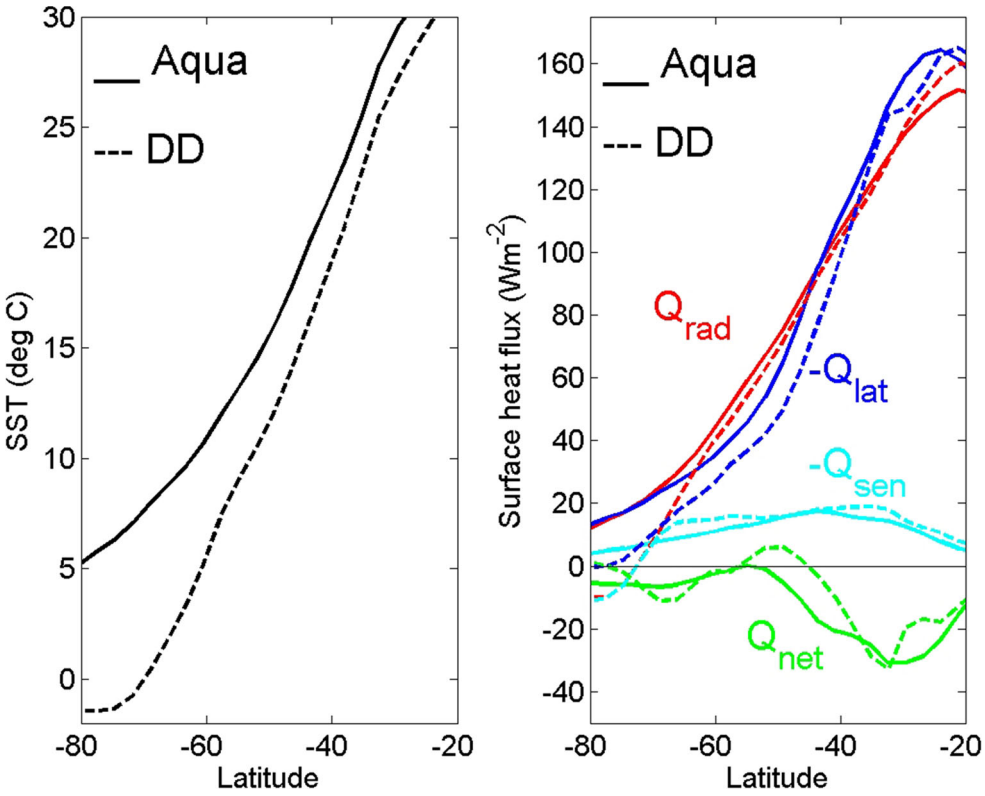

Fig. 3 (*Left panel*) SST and (*right panel*) net surface heat flux (Q_{net} in *green*, positive indicating heating of the ocean), net radiative heat gain (Q_{rad} in *red*, positive indicating heating of the ocean), sensible cooling ($-Q_{sen}$ in *light blue*, positive indicating cooling of the ocean), evaporative cooling ($-Q_{lat}$ in *dark blue*, positive indicating cooling of the ocean). In both panels, the continuous curves refer to the Aquaplanet experiment while the *dashed curves* are for the Double-Drake experiment

increase by a few degrees in the Double-Drake experiment compared to the Aquaplanet configuration (not shown). In the Southern Hemisphere, this meridional overturning circulation (hereafter the residual circulation) is thermally indirect and weaker than the wind driven Ekman cell as a result of a compensation from the parameterized eddy-driven circulation. The compensation is close to perfect in the Aquaplanet simulation but only partial in the Double-Drake experiment (not shown). The role of the ocean in warming the Northern Hemisphere relative to the Southern Hemisphere in such calculations and observations is discussed in Marshall et al. (2014).

The simulated annual mean net air-sea heat fluxes are shown in Fig. 3 (right panel) for both the Aquaplanet (green continuous lines) and Double-Drake (green dashed lines) geometry. Departures from zonal symmetry are very weak in these simulations, even in the Double-Drake experiments (not shown). We thus focus on the 40° S–60° S latitude band where the model ACC resides in both experiments. It is seen that in this latitude band, the Double-Drake experiment has a weak net heating of a few Wm^{-2} (centred on 45–55° S), while in the Aquaplanet geometry, the net air-sea heat flux is weak or, northward of 55° S, cools the upper ocean.

To explain this difference, the components of the net air-sea heat flux are also displayed in Fig. 3 (right panel). It is readily seen that, compared to the Aquaplanet experiment, the Double-Drake simulation has a slightly enhanced sensible cooling of the ocean (light blue curves) and weakened radiative heat gain (red curves). These components thus cannot explain the net heat gain seen in the ACC band in the Double-Drake experiment. The latter must result from a weaker surface evaporative cooling Q_{lat}, as confirmed by inspection of this quantity (dark blue curves). Averaged over the 45° S–55° S band, the change in Q_{lat} between the two simulations is found to be on the order of 13 Wm^{-2} while the corresponding change in SST is 4 K (Table 1). The implied sensitivity $13/4 \approx 3\ \mathrm{Wm}^{-2}\ \mathrm{K}^{-1}$ is weak compared to typical values found in climate models in the Northern Hemisphere (e.g., Frankignoul et al. 2004), but it is similar to that estimated for the Southern Ocean by Ferreira et al. (2015) and Hausmann et al. (2015). This likely reflects the planetary scale of the thermodynamic adjustment between SST and specific humidity in the near "aquaplanet" geometry of the Southern Ocean.

4 An idealized model of air-sea fluxes over the ACC

4.1 Model formulation

The results presented in Sections 2 and 3 make it clear that the heat source sustaining a net ACC heat gain is the radiative term Q_{rad}, since both sensible and latent heat flux are found to systematically cool the upper ocean. There are considerable uncertainties, however. The fraction of the net radiative heat gain realized as net heating over the ACC

Table 2 Model constants and parameters

Model constants	Name	Value (SI unit)
a	Earth's radius	6371 km
c_o	Specific heat capacity	4000 J kg^{-1} K^{-1}
l_v	Latent heat of vaporization	2.5×10^6 J kg^{-1}
ρ_a	Air density at sea level	1.2 kg m^{-3}
Model parameters	Name	Value (SI unit)
Q_{rad}	Net radiative heat gain	60 W m^{-2}
RH	Relative humidity of the marine boundary layer	0.8
C_E	Transfer coefficient for surface latent heat flux	1.5×10^{-3}
C_D	Transfer coefficient for surface momentum flux	1.5×10^{-3}
A_{ACC}	Surface area covered by the ACC	1.59×10^{13} m^2

The value for A_{ACC} and Q_{rad} are inferred from the data in Section 2. Other values are standard

is rather different in the reanalysis and the coupled model. To quantify this process, it is useful to define a heating efficiency η, thus:

$$\eta \equiv \frac{Q_{net}}{Q_{rad}} \tag{2}$$

such that, when $\eta = 1$, all the incoming solar radiation is realized as heating. Using the numbers in Table 1, $\eta = 28/59 \approx 50$ % for ACC-averaged NCEP-NCAR observations, $\eta = 4/67.5 = 6$ % for MITgcm (Double-Drake simulation) and $\eta = 0$ (no net heating)[1] in the MITgcm (Aquaplanet simulation).

To understand the processes responsible for this spread, we consider a simplified model for the heat budget of the upper branch of the residual circulation in the Southern Ocean based on the following assumptions:

- First, the previous two sections suggest that the main cooling mechanism is Q_{lat}, so we neglect the sensible heat flux. Given a radiative heat gain Q_{rad}, we attempt to predict $\eta \approx (Q_{rad} + Q_{lat})/Q_{rad}$, i.e.:

$$\eta \approx 1 - \frac{|Q_{lat}|}{Q_{rad}} \tag{3}$$

- Second, we neglect the lateral residual eddy heat fluxes in the mixed layer and consider a purely advective heat balance. This is clearly an idealization but it captures the leading order mixed-layer physics (see for example the high-resolution simulations in Abernathey et al. 2012).
- Finally, we assume the residual flow in the mixed layer to be a function of wind stress at the sea surface (e.g., Marshall J and Radko 2003).

[1]We have chosen to define $\eta > 0$ and set it to zero in absence of net heating.

These assumptions enable us to express the steady state mixed layer heat budget thus:

$$c_o \psi_b \frac{\partial T_m}{\partial y} = Q_{net} \tag{4}$$

in which y denotes the Northward coordinate, ψ_b is the mass transport streamfunction at the base of the mixed layer (see Eq. 11 in Marshall J and Radko 2003), T_m is the mixed layer temperature (= SST), and c_o is the specific heat capacity of the mixed layer. Although Eq. 4 is written in Cartesian coordinates to make clear the link with Marshall J and Radko (2003) Eq. 11, the calculations below have been carried out in spherical geometry (in the latter, the heat budget takes the form: $c_o \psi_b \frac{\partial T_m}{\partial \phi} = 2\pi a^2 \cos\phi \; Q_{net}$ where ϕ is latitude and a the Earth's radius). Note that the values of all model constants and parameters are listed in Table 2.

Equation 4 is coupled to a simplified expression for Q_{net}, namely:

$$Q_{net} = Q_{rad} - \rho_a C_E U l_v (1 - RH) q^\star(T_m, P) \tag{5}$$

in which we have used standard bulk formulae (air density ρ_a, transfer coefficient C_E, surface wind speed U, enthalpy of vaporization l_v, and relative humidity RH). The saturation-specific humidity $q^\star$ depends on surface temperature and also weakly on pressure P (the latter is set to a constant value of 1000 hPa enabling us to drop the pressure dependence in the following). Note that in Eq. 5, we have also neglected the dependence of the latent heat flux on air-sea temperature difference, consistent with our neglect of the sensible heat flux.

The coupled Eqs. 4–5 are further discretized on a meridional grid. Denoting by T_N and T_S, the value of T_m at the Northern and Southern boundary of the ACC, respectively, we approximate (4)–(5) as:

$$c_o \psi_b (T_N - T_S) = A_{ACC} Q_{net} \tag{6}$$

$$Q_{net} = Q_{rad} - \rho_a C_E U l_v (1 - RH) q^\star (\frac{T_N + T_S}{2}) \quad (7)$$

in which A_{ACC} is the surface area covered by the ACC, and Q_{net}, Q_{rad}, and ψ_b are averaged values representative of the ACC core. Finally, explicitly writing the dependence of the residual flow on surface wind stress τ_x, we have:

$$\psi_b = \psi_b(\tau_x) \quad (8)$$

with

$$\tau_x = \rho_a C_D U^2 \quad (9)$$

in which C_D is a transfer coefficient for the surface momentum flux.

Relations (6–9) allow a prediction of the evaporative cooling over the ACC, and hence η, given U, T_S, Q_{rad}, and knowledge of the functional dependence of ψ_b upon windstress (discussed below). Our reference choice of parameters is listed in Table 2. The Appendix gives details of the method used to solve the model and also presents an analytical solution for a linearized version of the Clausius-Clapeyron relation used in computing $q^\star(T)$.

4.2 Model results

First, let us analyze the conditions under which the model predicts no heating at all ($Q_{net} = 0$, i.e., $\eta = 0$), even though a residual ocean flow is present ($\psi_b \neq 0$). From Eq. 7, this occurs when net radiative heating equals latent heat loss:

$$Q_{rad} = \rho_a C_E U l_v (1 - RH) q^\star(T_S), \quad (10)$$

in which we have further used the fact that if $Q_{net} = 0$, Eq. 6 requires $T_N = T_S$ if $\psi_b \neq 0$. Eq. 10 is inferred solely on considerations of air-sea interactions. It predicts, as a function of surface wind speed (U) and SST (T_S), whether the ACC will experience heat gain or heat loss. The zero heating curve is plotted in Fig. 4 as a function of windstress and T_S for the standard values of parameters listed in Table 2. Note that windstress is plotted rather than wind speed, making use of Eq. 9. Net heating of the ACC is predicted when, for a given value of T_S, the winds are not too strong, resulting in evaporative cooling which is less than the specified radiative heating. Conversely, at a given value of wind speed, the ACC will experience heat loss if the surface temperature (and thus the evaporative cooling) exceeds a critical value. It is seen that for realistic values of windstress ($\tau_x \approx 0.2$ Nm^{-2}), the value of T_S separating net cooling from net heating is very high (≈ 7 °C), supporting the view that in the real world (remember from Section 2 that SST on the Southern edge of the ACC is $T_s \approx 1$–2 °C) the Southern Ocean experiences net heating. Indeed, Fig. 4 suggests that it would be very difficult to envisage an ACC in which there

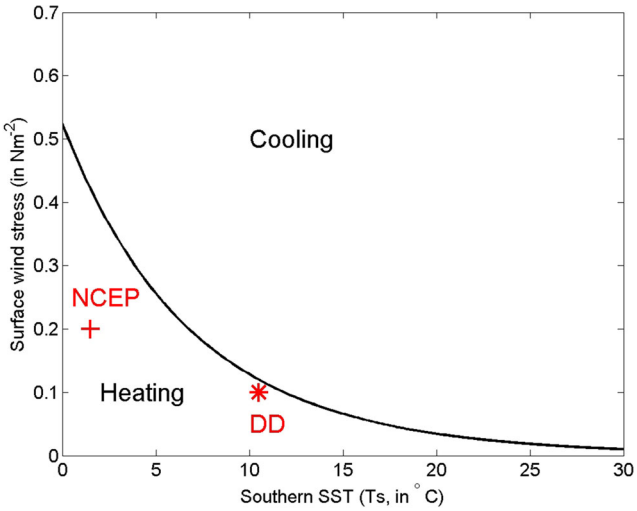

Fig. 4 Model prediction, i.e. Eq. 10 and Table 2, for the surface wind stress (τ_x in Nm^{-2}) at which, for a given SST at the Southern edge of the ACC (T_S in °C), the net surface heating of the ACC vanishes. Typical values for the present climate are $T_s \simeq 1 - 2$ °C and $\tau_x \approx 0.2\ Nm^{-2}$ (inferred from NCEP-NCAR data in Section 2), placing the ACC in the region of heating (red cross). The Double Drake (DD) simulation, with $T_s \approx 10.5$ °C and $\tau_x = 0.1$ Nm^{-2}, is much closer to the zero heating curve (red asterisk)

is net cooling, unless the surface temperature or the surface winds increase considerably (the location of the ACC, based on NCEP-NCAR data, is indicated with a red cross in this figure).

Were surface wind speed and temperature to obey (10) exactly, no heating or cooling would occur and an isothermal layer would develop in the mixed layer over the range of latitude $\Delta\phi$. At depth, this isothermal layer would slope downward and equatorward, sandwiched, from below by water at temperature $T < T_S$ and above by water at temperature $T > T_S$. To our knowledge, this "isothermal ACC limit" has not been observed or seen in climate models.

Let us now turn to a prediction of the heating efficiency η defined in Eq. 3. As discussed in Section 4.1, we must first specify how the residual flow depends on surface winds—Eq. 8. Motivated by the results in Abernathey et al. (2012), which showed a linear dependence of ψ_b (strictly speaking, the maximum of their "upper MOC cell" see their Fig. 5), we consider,

$$\psi_b = \mu \tau_x. \quad (11)$$

As discussed in Abernathey et al. (2012), the exact value of μ is sensitive to surface boundary conditions and they found $\mu = 25 \times 2.6 = 65$ Sv/Nm^{-2} (fixed surface heat flux)[2] and $\mu = 25 \times 4.5 = 112.5$ Sv/Nm^{-2} (restoring boundary condition). The latter case is more relevant to the model used here so we choose $\mu = 112.5$ Sv/Nm^{-2} in the following. This

[2]The numbers are taken from Table 2 in Abernathey et al. (2012), after multiplication by 25 to account for domain size.

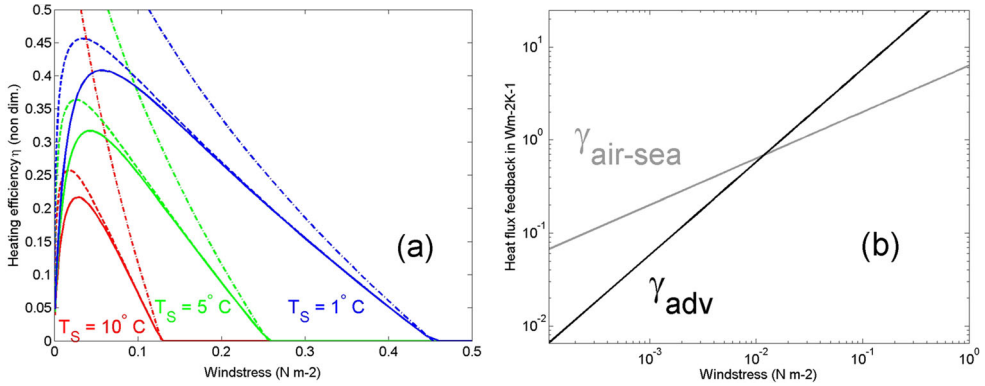

Fig. 5 Model prediction for **(a)** heating efficiency η (Eq. 2, *continuous lines*) and η_S (Eq. 13, *dash-dotted lines*) as a function of surface wind stress for various values of T_S (indicated on the plot). The *dashed lines* correspond to the linearized calculation (12) described in the Appendix. Panel **b** shows the heat flux feedbacks γ_{adv} (Eq. 15, *black*) and $\gamma_{air-sea}$ (Eq. 14, *gray*, both in $\mathrm{Wm^{-2}\ K^{-1}}$) as a function of surface wind stress when T_S = 1 °C. Note the log scale in **(b)**. The standard parameters' values listed in Table 2 were used for both panels

value likely overestimates the sensitivity of ψ_b to the wind-stress since it applies to the maximum streamfunction, not its value at the base of the mixed layer.

Figure 5a illustrates the implied dependence of η upon surface wind stress and T_S. One observes a simple monotonic dependence of η on T_S, with decreasing efficiency as T_S is increased (continuous lines of different colors with T_S increasing from blue to red). Note, however, that for a given value of T_S, a more complex dependence of η on wind speed is observed: η first increases with wind stress, until a maximum is reached, then decreases with wind stress until the boundary (10) is crossed.

To understand this dependence, we have computed an analytical solution to the model by linearizing the Clausius-Clapeyron relation used in the calculation of $q^\star$. As detailed in the Appendix, this solution takes the form,

$$\eta = \eta_S/(1 + \gamma_{air-sea}/\gamma_{adv}) \tag{12}$$

in which

$$\eta_S = 1 - \rho_a C_E U l_v (1 - RH) q^\star(T_S)/Q_{rad} \tag{13}$$

is the heating efficiency obtained if the SST across the ACC were uniform and equal to T_S, and

$$\gamma_{air-sea} = \rho_a C_E U l_v (1 - RH) \left(\frac{\partial q^\star}{\partial T}\right)_{T=T_S} \tag{14}$$

$$\gamma_{adv} = \frac{2 c_o \psi_b}{A_{ACC}} \tag{15}$$

are two heat flux-feedbacks (in $\mathrm{Wm^{-2}\ K^{-1}}$) associated with surface evaporation ($\gamma_{air-sea}$) and oceanic advection (γ_{adv}). The evaporative feedback has often been used in climate studies (see for example the comprehensive study in Frankignoul et al. 2004), and the concept has also been applied to analysis of the ocean's mixed layer heat budget (e.g., Greatbatch et al. 2007). The advective feedback has been less often considered. In the context of this model, it measures by how much the cooling due to advection increases per degree increase in SST over the ACC. Like $\gamma_{air-sea}$, γ_{adv} represents a negative feedback on SST anomaly developing over the ACC: a warm anomaly, for example, corresponds to a larger SST gradient across the ACC at fixed T_S, and hence a larger cooling by advection.[3]

The approximate solution (dashed lines in Fig. 5a) compares rather well with the full solution (continuous lines in Fig. 5a) and can thus be used to understand the dependence of η on wind stress. The reference efficiency η_S can be thought of as the maximum efficiency possible because it corresponds to the case where, at a given wind speed, the ACC maintains a uniform SST equal to T_S, which is the lowest possible temperature given our assumptions. As seen from Eqs. 12 and 15, it corresponds to the limit case of a mixed layer with an infinite heat capacity ($\eta \to \eta_S$ when $c_o \to \infty$). In this limit, the ACC is able to absorb solar radiation without changing its SST. This maximum efficiency (η_S, dash-dotted lines in Fig. 5a) decays linearly with wind speed, from a value of unity at zero wind speed to zero when Eq. 10 is satisfied. It also decays monotonically with increasing T_S, as is evident from the definition (13) and the fact that $q^\star$ increases monotonically with T_S.

Starting from the reference case just described, suppose that, at a given wind speed, one lowers the heat capacity of the mixed layer to a finite value. Then, to reach a steady state, the radiative heat gain must now be exactly balanced by a cooling mechanism. The SST of the ACC will then become under the control of advection and surface

[3] Expressed differently, because T_S is prescribed, a change of SST of 1 K over the ACC ($= (T_N + T_S)/2$) is equivalent to a 2 K increase in T_N and a strengthening of the SST gradient by 2 K across the ACC. This term is thus, within the limitations imposed by the coarse meridional discretization used, the analog to a $\overline{v}\partial T'/\partial y$ term in a continuous model.

evaporative cooling, rather than being fixed to T_S. If, at the wind speed considered, the sensitivity of SST to advection is greater than that to evaporation (as measured by a ratio $\gamma_{adv}/\gamma_{air-sea} \geq 1$), then only a weak increase in SST will result since cooling of the ocean by advecting cold water from the South will alleviate the need for an increase in evaporation. In this case, η will not deviate too much from η_S. Conversely, if the sensitivity to advection is weaker than that to evaporative cooling, the effect of advection will be weak and the ACC will need to warm up so that evaporation can increase sufficiently to allow equilibrium. The heating efficiency of the ACC is thus ultimately sensitive to the ratio $\gamma_{adv}/\gamma_{air-sea}$, in agreement with Eq. 12.

The bell-shape dependence in Fig. 5a can simply be understood from the previous thought experiment. For the particular choice considered in Eq. 11, $\gamma_{air-sea}$ increases more slowly with wind speed (linear) than γ_{adv} (quadratic)—see Fig. 5b. Hence, at low wind speed (or low windstress), the efficiency η in Fig. 5a (continuous curves) is dramatically reduced compared to η_S (dash-dotted curves). As the wind speed increases, γ_{adv} eventually becomes as large or greater than $\gamma_{air-sea}$, and η in Fig. 5a becomes closer to η_S.

The model allows one to understand the range of values obtained for η in Sections 2 and 3. For both the real-world and the Double-Drake simulation, a significant residual circulation exists so the model (11) is appropriate. NCEP-NCAR data suggested a high efficiency (50 %), which, according to the model, can only be found when the SST at the Southern edge of the ACC is on the order of a few °C (Fig. 5a), as observed. For realistic conditions ($\psi_b = 15$ Sv, $U = 7$ ms^{-1}, and $T_S = 1.1$ °C), one obtains $\gamma_{adv} \approx 6$ Wm^{-2} K^{-1} and $\gamma_{air-sea} \approx 2$ Wm^{-2} K^{-1}. The heating efficiency in the real world is thus expected to be $\eta \approx 3\eta_S/4$, and is thus indeed close to its maximum possible value.

The fact that the Double-Drake simulation experiences net heating at all might be surprising from Fig. 4, since the latter suggests that with $T_S > 7$ °C, as occurs in this simulation (Fig. 3, left panel, shows that the SST is ≈ 10 °C at 60° S, which is the value of T_S relevant in this case), net cooling should be found for $\tau_x \approx 0.2$ Nm^{-2}. The surface wind stress is actually about half this value in the Double-Drake simulation (not shown), putting its ACC on the edge of the heating domain in Fig. 4 (see red asterisk in this figure). The large difference between this simulation and the real world is likely due to the large differences in η_S, as a result of large differences in T_S, rather than differences in $\gamma_{air-sea}$ or γ_{adv}.

The Aquaplanet simulation has $\psi_b \approx 0$ for a realistic surface wind stress, and the net cooling found in Table 1 must be opposed by a warming through lateral residual eddy heat fluxes (the "diapycnal eddy heat fluxes" in the terminology of Marshall J and Radko 2003), which have been neglected here. Our model is thus less relevant to this case.

5 Discussion and conclusions

We have seen that net sea surface heat gain by the ACC is sustained by radiative fluxes Q_{rad} (the sum of solar heat gain and net long wave cooling) and not, as has been suggested in previous studies (Taylor et al. 1978; Speer et al. 2000), by heat gain through sensible heat flux at the air-sea interface as a result of warm air advection by the atmosphere. As Table 1 summarizes, a broad range of climate states supports this view. It is also confirmed by the fact that a model without any sensible heating can sustain a realistic net heat gain by the ACC as shown in Section 4. The model further suggests that the fraction η of the net radiative heat gain realized as net ACC heating is set by (i) the SST at the Southern edge of the ACC and (ii) the relative strength of oceanic advection and surface latent heat flux feedbacks, as measured by the parameters γ_{adv} and $\gamma_{air-sea}$ in Section 4. These parameters both depend on surface wind speed and measure whether advection of cold water from the South or cooling by surface evaporation control the surface heat balance. Strong advection by the residual flow and weak evaporative feedback favor net ACC heating. Observations suggest that $\gamma_{adv} \simeq 6$ Wm^{-2} K^{-1} and $\gamma_{air-sea} \simeq 2$ Wm^{-2} K^{-1}, putting the ACC in the warming regime.

One important caveat to our study is that it might only be relevant to the zonally (or streamline) averaged heat budget. As Fig. 2 suggests, and in agreement with the suggestions in Taylor et al. (1978) and Speer et al. (2000), sensible heating of the ACC is found in the annual mean over the Atlantic and Indian sectors of the Southern Ocean. The NCEP-NCAR dataset used in Fig. 2 suggests that the associated heating (light blue curve) is modest in comparison to the heat gained by radiative processes (red curve). However, considering the large uncertainties in heat fluxes in the Southern Ocean (e.g., Badin and Williams 2010), one cannot rule out the possibility that sensible heat gain can be locally important when considering zonal asymmetries in the annual mean mixed layer heat budget.

The model developed in Section 4 has applications outside the ACC, in particular to regions where surface oceanic flows are poleward instead of equatorward. It can be applied directly to the Northern Hemisphere which, in a zonally averaged sense, has poleward flow in the mixed layer at the latitude of the Jet Stream. With T_S now interpreted as a subtropical SST ($\simeq 20$ °C), and also considering that $\tau_x = 0.1$ Nm^{-2} is more relevant to the Northern Hemisphere case, inspection of Fig. 4 suggests a large net cooling, in agreement with observations.

Finally, returning to high southern latitudes, the fact that the Southern Ocean experiences net heat gain has interesting implications for the oceanic and atmospheric residual circulations (Fig. 6). In the Southern Hemisphere, their surface branches are both directed toward the tropics: air parcels gain heat (or enthalpy) through turbulent air-sea fluxes, and water parcels through net radiation (Fig. 6a). This contrasts sharply with the Northern Hemisphere (Fig. 6b) where the surface branches of the circulation circulate in opposite ways. Air parcels originating from high latitudes gain heat through turbulent heat fluxes at low levels, as in the Southern Hemisphere, but these fluxes are so large that they lead to a cooling of ocean parcels in the net in the Northern Hemisphere. In the framework of our simple model (Section 4, see also the previous paragraph), this large increase in surface turbulent heat flux is primarily controlled by the larger sea surface temperature at the southern boundary of the inflow in the Northern Hemisphere compared to that occurring in the Southern Hemisphere, which directly reflects the different sense of circulation of the upper residual flow (poleward vs equatorward). The different geometry of the basins ("gyre" in the North as opposed to "channel" in the South) also further leads to differences in the heat flux feedback parameter $\gamma_{air-sea}$: the greater thermodynamic imbalance associated with the presence of the continents in the Northern Hemisphere leads to a greater value of this parameter in the Northern Hemisphere compared to the Southern Hemisphere. Both air-sea interactions and circulation thus favour net surface heating of the Southern Ocean while they favor net surface cooling in Northern basins.

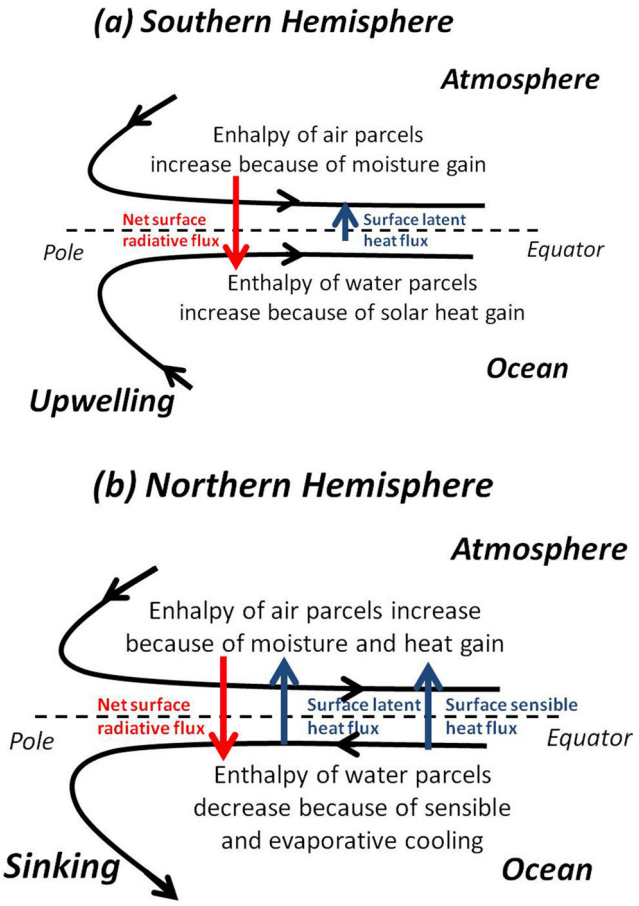

Fig. 6 Schematic of the surface branches of the oceanic and atmospheric residual circulations in a height/latitude plane for **a** the Southern and **b** Northern Hemispheres. The net surface radiative heat gain is depicted by a *red arrow* while sensible and latent cooling by a *blue arrow*. Note the different length of the turbulent heat flux arrows in **a** and **b**, reflecting the reduction of the evaporative and sensible cooling by advection of cold water. Enthalpy is used here as opposed to heat to include, for the atmosphere, the source due to evaporation

Acknowledgments Discussions with Aaron Donohoe (MIT) and David Ferreira (Reading University) helped greatly in the preparation of this manuscript. David Ferreira also kindly provided the MITgcm outputs. JM acknowledges support from NSF's 'Frontiers in Earth System Dynamics' program. Finally, both authors would like to thank Richard Greatbatch for countless discussions and enjoyable encounters over many years. It is a pleasure to dedicate this study to Richard's 60th birthday.

Appendix: Model Solving

The model Eqs. 6→9 allows a prediction of the evaporative cooling over the ACC, and hence η, given U, T_S, Q_{rad} and knowledge of the functional dependence of ψ_b upon wind-stress. Technically, we prescribe T_s, the SST at the poleward edge of the ACC, the net radiative heating Q_{rad}, and the surface wind speed U, and solve the following equation for the temperature T_N on the equatorward flank of the ACC,

$$c_o \psi_b (T_N - T_S) = A_{ACC} \left[Q_{rad} - \rho_a C_E U l_v (1 - RH) q^\star \left(\frac{T_N + T_S}{2} \right) \right]. \tag{16}$$

Once T_N is known, the net heating over the ACC, and hence η, can be estimated from Eq. 7.

Analytical solution

It is useful to seek analytical solutions by linearizing the Clausius-Clapeyron equation required to find $q^\star$. Using a Taylor expansion near $T = T_S$, we have,

$$q^\star \left(\frac{T_N + T_S}{2} \right) \approx q^\star(T_S) + \left(\frac{T_N - T_S}{2} \right) \Gamma_S \tag{17}$$

in which

$$\Gamma_S = \left(\frac{\partial q^\star}{\partial T} \right)_{T=T_S}. \tag{18}$$

Using this, Eq. 16 can be rewritten as,

$$\left(\frac{c_o\psi_b}{A_{ACC}} + \frac{\rho_a C_E U l_v (1-RH)\Gamma_S}{2}\right)(T_N - T_S) = Q_{rad} - \rho_a C_E U l_v (1-RH) q^\star(T_S) \quad (19)$$

The efficiency η can then be computed from

$$\eta = \frac{c_o\psi_b(T_N - T_S)}{A_{ACC}\,Q_{rad}} \quad (20)$$

which, after using Eq. 19 and the definition of η_S in Eq. 13, can be expressed as,

$$\eta = \eta_S \frac{c_o\psi_b/A_{ACC}}{c_o\psi_b/A_{ACC} + \rho_a C_E U l_v (1-RH)\Gamma_S/2} \quad (21)$$

$$= \eta_S \frac{2c_o\psi_b/A_{ACC}}{2c_o\psi_b/A_{ACC} + \rho_a C_E U l_v (1-RH)\Gamma_S} \quad (22)$$

$$= \eta_S \frac{\gamma_{adv}}{\gamma_{adv} + \gamma_{air-sea}} \quad (23)$$

in which $\gamma_{air-sea}$ and γ_{adv} are defined in Eqs. 14 and 15, respectively. This yields Eq. 12 in Section 4.2.

References

Abernathey R, Marshall J, Ferreira D (2012) The Dependence of Southern Ocean Meridional Overturning on Wind Stress. J Phys Oce 41:2261–2278

Badin G, Williams RG (2010) On the Buoyancy Forcing and Residual Circulation in the Southern Ocean: The Feedback from Ekman and Eddy Transfer. J Phys Oce 40:295–310

Csanady GT (2001) Air-sea interaction, Cambridge University Press, 239 pp

Czaja A, Marshall J (2006) The partitioning of the poleward heat transport between ocean and atmosphere. J Atm Sci 63:1498–1511

Enderton D, Marshall J (2009) Explorations of Atmosphere-Ocean-Ice Climates on an Aquaplanet and Their Meridional Energy Transports. J Atm Sci 66:1593–1611

Ferreira D, Marshall J, Campin J (2010) Localization of Deep Water Formation: Role of Atmospheric Moisture Transport and Geometrical Constraints on Ocean Circulation. J Clim 23:1456–1476

Ferreira D, Marshall J, Rose B (2011) Climate determinism revisited: multiple equilibria in a complex climate model. J Clim 24:992–1012

Ferreira D, Marshall J, Bitz C, Solomon S, Plumb A. (2015) Antarctic ocean and sea ice response to ozone depletion: a two-timescale problem. J Clim 28(3):1206–1226

Frankignoul C, Kestenare E, Botzet M, Carril AF, Drange H, Pardaens A, Terray L, Sutton R (2004) An intercomparison between the surface heat flux feedback in five coupled models, COADS and the NCEP reanalysis. Clim Dyn 22:373–388

Ganachaud A, Wunsch C (2000) Improved estimates of global ocean circulation, heat transport and mixing from hydrographic data. Nature 408:453–456

Gnanadesikan A (1999) A simple predictive model for the structure of the pycnocline. Science 283(5410):2077–2079

Greatbatch RJ, Zhang X, Eden C, Olbers D (2007) The possible role in the ocean heat budget of eddy-induced mixing due to air-sea interaction. Geophys Res Let 34:L07604. doi:10.1029/2007GL029533

Grist JP, Josey SA (2003) Inverse analysis adjustment of the SOC air-sea flux climatology using ocean heat transport constraints. J of Clim 16:3274–3295

Hausmann U, Czaja A, Marshall J (2015) Air-sea damping rates of sea surface temperature anomalies in the Southern ocean, submitted to J. Clim

Howe NJ, Czaja A (2009) A New Climatology of Air-Sea Density Fluxes and Surface Water Mass Transformation Rates Constrained by WOCE. J Phys Oce 39(6):1432–1447

Isemer H, Hasse L (1987) The Bunker Climate Atlas of the North Atlantic Ocean, vol 2: Air-Sea interactions, Springer Verlag, 252 pp

Kalnay E, et al. (1996) The NCEP/NCAR 40-year reanalysis project. Bull of the AMS 103(18):567–18. 589

Marshall D (1997) Subduction in an eddying ocean. J Mar Res 55:201–222

Marshall J, Adcroft A, Hill C, Perelman L, Heisey C (1997) Finite-volume, incompressible Navier Stokes model for studies of the ocean on parallel computers. J of Geophys Res Oce 102(C3):5753–5766

Marshall J, Radko T (2003) Residual mean solutions for the Antarctic Circumpolar Current and its associated overturning circulation. J Phys Oce 33:2341–2354

Marshall J, Adcroft A, Campin JM, Hill C (2004) Atmosphere-ocean modeling exploiting fluid isomorphisms. Monthly Weather Review 132(12):2882–2894

Marshall J, Speer K (2012) Closure of the meridional overturning circulation through Southern Ocean upwelling. Nat Geosci 5(3):171–180

Marshall J, Donohe A, Ferreira D, McGee D (2014) The oceans role in setting the mean position of the Inter-Tropical Convergence Zone. Clim Dyn 42(7-8):1967–1979

Maximenko N, Niiler P, Rio MH, Melnichenko O, Centurioni L, Chambers D, Zlotnicki V, Galperin B (2009) Mean dynamic topography of the ocean derived from satellite and drifting buoy data using three different techniques. J Atm Ocean Tech 26:1910–1919

Molteni F (2003) Atmospheric simulations using a GCM with simplified physical parametrizations. I: model climatology and variability in multi-decadal experiments. Clim Dyn 64:175–191. doi:10.1007/s00382-002-0268-2

Speer K, Rintoul SR, Sloyan B (2000) The diabatic Deacon cell. J Phys Oce 30:3212–3222

Taylor HW, Gordon AL, Molinelli E (1978) Climatic characteristics of the Antarctic Polar front zone. J Geophys Res 83(C9):4572–4578

Toggweiler JR, Samuels B (1998) On the ocean's large-scale circulation in the limit of no vertical mixing. J Phys Oce 28(9):1832–1852

Walin G (1982) On the relation between sea-surface heat flow and thermal circulation in the ocean. Tellus 34:187–195

Wunsch C, Ferrari R (2004) Vertical mixing, energy, and the general circulation of the oceans. Ann Rev Fluid Mech 36:281–314